

# DIELECTRIC PROPERTIES, AC ELECTRICAL CONDUCTIVITY AND ELECTRIC MODULUS PROFILES OF HEMATITE ( $\alpha$ -Fe<sub>2</sub>O<sub>3</sub>) NANOPARTICLES

S. Anand<sup>1</sup>, V. Maria Vinosel<sup>2</sup>, M. Asisi Jenifer<sup>3</sup>, S. Pauline<sup>4</sup>

<sup>1,2,3,4</sup>Department of Physics, Loyola College, Chennai – 600034, India

\*\*\*

**Abstract** – Hematite nanoparticles ( $\alpha$ -Fe<sub>2</sub>O<sub>3</sub>) were prepared via facile hydrothermal technique. X-ray diffraction pattern confirmed that the synthesized nanoparticles crystallized with rhombohedral lattice structure. The functional groups were determined using FTIR spectrum which clearly confirms the formation of  $\alpha$ -Fe<sub>2</sub>O<sub>3</sub> nanoparticles. The morphological and energy dispersive X-ray analysis were carried out using EDAX coupled with high resolution scanning electron microscope (HRSEM) analysis. Nanocrystalline  $\alpha$ -Fe<sub>2</sub>O<sub>3</sub> with grain size of 35 nm has been studied in dielectric spectroscopy. Impedance, relative dielectric permittivity, loss tangent and electric modulus have been measured in the frequency range 50 Hz – 5MHz at temperatures between 323 K and 473 K.

**Keywords:**  $\alpha$ -Fe<sub>2</sub>O<sub>3</sub>, FT-IR, Dielectric Studies, AC conductivity, Electric modulus

## 1. INTRODUCTION

Magnetic particles have attracted significant research interest in recent years due to their wide collection of applications in as an oxygen evolution, microwave absorption, magnetic recording, contrast agent and electrochemical energy storage devices [1]. Hematite is the most stable iron oxide with high resistance to corrosion, low cost, and it is also biocompatible, environmentally friendly and non-toxic. Hematite ( $\alpha$ -Fe<sub>2</sub>O<sub>3</sub>) crystallized in the rhombohedral system space group R-3c with n-type semiconducting properties (2.1 eV band gap) [2]. There are large numbers of methods, such as sol-gel, precipitation, mechanochemical, solvothermal, thermal decomposition, hydrothermal, has been established to prepare numerous hematite nanostructures [3-7].

The research and development in the dielectric, piezoelectric and ferroelectric materials have increased due to the availability of new materials with good physical properties in different form like bulk single crystals, ceramics, thin films, nanotubes, nanowires etc [8]. These materials can find application in the field of sensors, transducers, micro-electromechanical systems, microwave tuners, capacitors, electro-optic modulators etc. [8-10]. The electrical properties of dielectric materials are usually

described in terms of dielectric constant. In the case of alternating fields the dielectric constant depends on the frequency of the applied field and temperature, which define the state of material. These dielectric materials are typically insulators where advantage is taken of their very high resistivity and low eddy currents in fabricating electrical and electronic devices. In this study,  $\alpha$ -Fe<sub>2</sub>O<sub>3</sub> nanoparticles were prepared by hydrothermal method and studied its structural, magnetic and dielectric properties.

## 2. EXPERIMENTAL

### 2.1 Preparation of $\alpha$ -Fe<sub>2</sub>O<sub>3</sub> nanoparticles

Hematite ( $\alpha$ -Fe<sub>2</sub>O<sub>3</sub>) nanoparticles were synthesized by a facile hydrothermal method. In a typical preparation procedure, 1M of FeCl<sub>3</sub>.6H<sub>2</sub>O was dissolved in 40 ml deionized (DI) water. Then 1M of Sodium Hydroxide was added into above solution. The mixture was transferred into a 100 ml Teflon-sealed autoclave and hydrothermally treated at 220°C for 5 h. The precipitate was collected and washed several times using deionized water and ethanol. Then the product was dried at 60°C for 12 h and annealed at 600°C for 2h.

## 3. RESULTS AND DISCUSSION

### 3.1 Powder XRD analysis

The crystal structure of the as prepared samples were determined by X-ray diffraction patterns obtained in the 2 $\theta$  range of (20°) to (70°) with (Cu K $\alpha$ ) radiation ( $\lambda$  = 1.5406 Å). The XRD pattern of hematite nanoparticle is shown in fig.1. In the XRD pattern of  $\alpha$ -Fe<sub>2</sub>O<sub>3</sub> nanoparticles, the diffraction peaks are present at 24.2, 33.4, 35.7, 41.2, 49.8, 54.3, 57.7, 62.8 and 64 that represent the (012), (104), (110), (113), (024), (116), (018) and (300) crystal planes. All the diffraction peaks are indexed to rhombohedral crystal phase of  $\alpha$ -Fe<sub>2</sub>O<sub>3</sub> (hematite, JCPDS no.33-0664) without the presence of other diffraction peaks from any impurities. The strong, sharp and narrow diffraction peaks showed that the as-synthesized product was well crystallized. The average

crystallite size (D) was calculated based on 104 peaks by applying well known Scherrer formula as 35nm range.

$$D = K\lambda / \beta \cos\theta$$

where, D is the crystallite size, K is the shape factor,  $\beta$  is the full width at half maximum,  $\lambda$  is the X-ray wavelength and  $\theta$  is the Bragg angle.

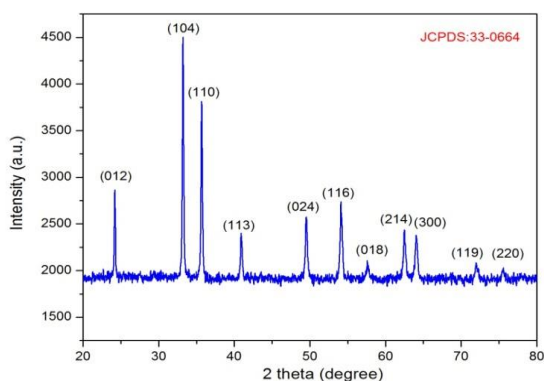


Figure 1: XRD pattern of hematite ( $\alpha$ -Fe<sub>2</sub>O<sub>3</sub>) nanoparticles

### 3.2 FTIR spectroscopy analysis

The functional group formation of  $\alpha$ -Fe<sub>2</sub>O<sub>3</sub> nanoparticles was further confirmed by FTIR spectroscopy. Fig.2 shows FTIR spectrum of as formed  $\alpha$ -Fe<sub>2</sub>O<sub>3</sub> sample at room temperature. The spectrum shows two intrinsic stretching vibration bands of Fe-O at 563 and 475 cm<sup>-1</sup>. The absorption peak observed at 3434 cm<sup>-1</sup> in the sample could be assigned to O-H stretching due to physically adsorbed water.

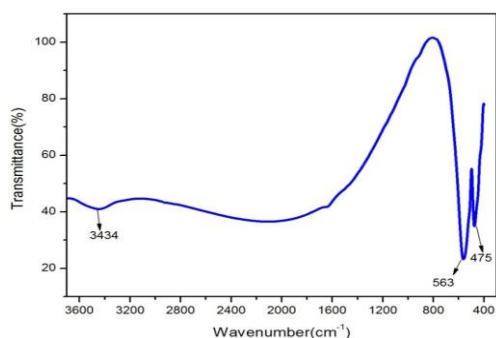


Figure 2: FTIR spectrum of hematite ( $\alpha$ -Fe<sub>2</sub>O<sub>3</sub>) nanoparticles

### 3.3 HRSEM and EDX analysis

The surface morphology and the elemental composition of hematite nanoparticles were recorded using

FEI Quanta FEG 200F model high resolution scanning electron microscope equipped with energy dispersive X-ray (EDX) instrument. Fig.3 (a) represents the surface morphology of hematite nanoparticles. The low-magnification HRSEM shows that the precursor is composed of high-yield uniform spheres shape.

Fig. 3(b) shows the EDX spectrum for the synthesized particles which clearly indicates that hematite structure is composed of only Fe and O. The data confirms the high purity of the as-synthesized sample.

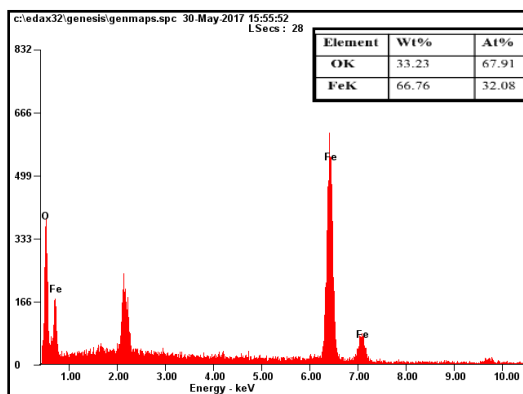
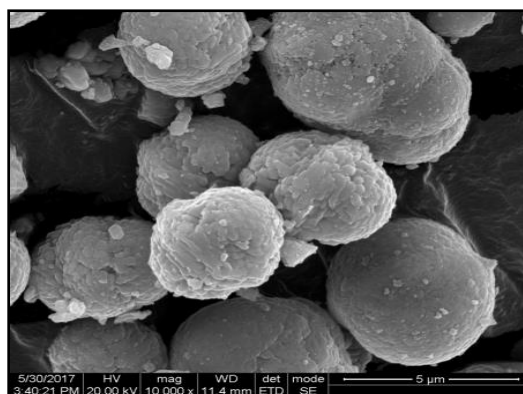


Figure 3(a): HRSEM image and 3(b) EDX spectrum of hematite ( $\alpha$ -Fe<sub>2</sub>O<sub>3</sub>) nanoparticles

### 3.4 Dielectric Properties

Dielectric constant  $\epsilon'$  is calculated from the measurement of capacitance value which can be obtained using the following equation,

$$\epsilon_r = \frac{C.d}{\epsilon_0 A}$$

Where, C is the capacitance, d is thickness and A is area of the sample,  $\epsilon_0$  is the permittivity of free space and its value is

$8.85 \times 10^{-12}$  F/m. Dielectric constant versus frequency for a sample is shown in fig.4(a) and is found to decrease with increasing frequency. This is because of polarization mechanism with applied frequency. For the frequency between 1 kHz and 1 MHz, the total contribution of polarization arises from electronic displacement, ionic displacement, dipole orientation and space charge displacement.

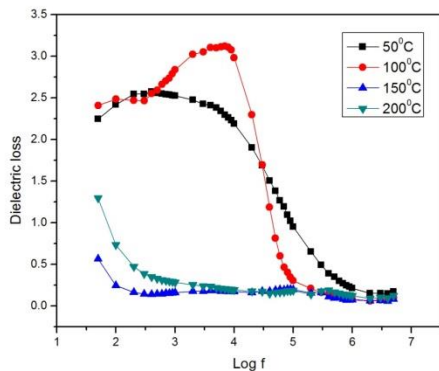
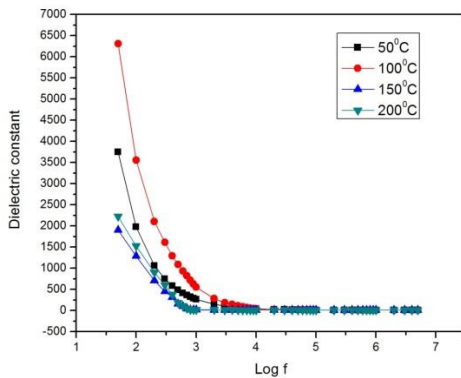


Figure 4: (a) Variation of dielectric constant and 4(b) dielectric loss with frequency

The imaginary part of permittivity or dielectric loss ( $\epsilon''$ ) is obtained from the value of dissipation factor D. Dielectric loss ( $\epsilon''$ ) versus frequency is shown in fig.4 (b) and is decreasing with increasing frequency, which shows the ability of these materials to be used for high frequency application. Loss is found to be a maximum at mid frequency region for 50 and 100° C which is a result of dipole polarization. This polarization depends on the atomic, interfacial and electronic polarizations. At higher frequencies the major contribution is due to the electronic polarization. The contribution of space charge polarization due to oxygen ion vacancies increases the dielectric loss at all temperatures [11-12].

### 3.5 Impedance

To understand the electrical behavior of prepared hematite nanoparticles, the impedance analysis is a powerful and best tool. The ferromagnetic materials consist of grains as well as grain boundaries. The impedance analysis helps to understand the conductive and/or resistive properties of a material [13]. The real part ( $Z'$ ) and imaginary part ( $Z''$ ) of the impedance can be represented as

$$Z' = Z_{\text{Real}} = |Z| \cos \theta \text{ and } Z'' = Z_{\text{Imaginary}} = |Z| \sin \theta$$

The variation in real impedance has been analyzed as a function of frequency, as shown in Figure 5(a). It can be observed that, as the frequency of the applied field is increased, the magnitude of the impedance decreases. A similar trend for imaginary ( $Z''$ ) part of the impedance with the applied frequency is shown in Fig.5(b). The AC conductivity and impedance have an inverse relation with each other. Our experimental results also prove that the impedance has a good agreement with the AC conductivity.

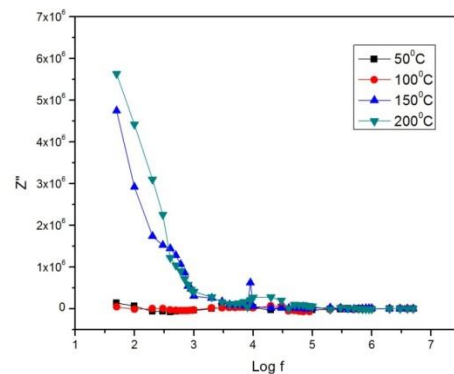
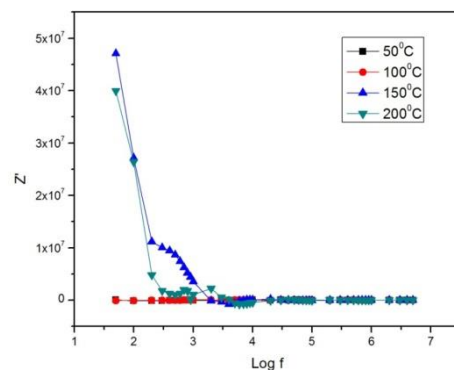


Figure 5: (a) Variation of the real part and 5(b) imaginary part of impedance with frequency

### 3.6 AC conductivity

AC conductivity ( $\sigma_{ac}$ ) studies of the synthesized sample have been carried out over a frequency range of 50 Hz to 5 MHz in the temperature range of 50 °C to 200 °C. The AC conductivity is calculated from dielectric data using the relation:

$$\sigma_{ac} = \omega \epsilon_0 \epsilon' \tan \delta$$

Where  $\sigma_{ac}$  is permittivity of free space and  $\omega$  is the angular frequency. The ac conductivity increased with increasing applied frequency is shown on fig.6. Generally, the electrical conductivity is directly related with the obtainable amount of free charge carriers and their mobility. The ac conductivity is affected by the mobile charge carriers.

According to an ion-hopping mechanism, the ionic conduction of the  $\alpha$ -Fe<sub>2</sub>O<sub>3</sub> results from the migration of exchangeable channels and cavities of the grains. As the mobile charge carriers hops to a new position, from its original position, it faces some displacements between the two minimum potential energy states. This may be because of the polarization of dipoles i.e. the dipoles rotate between the equivalent equilibrium positions.

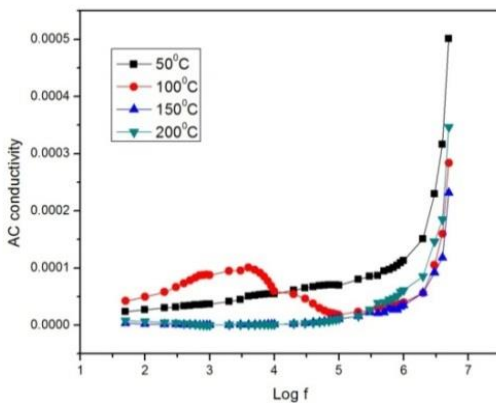


Figure 6: Variation of AC conductivity with frequency

### 3.7 Electric Modulus

The electric modulus is calibrated to analyze the dependency of the frequency for the interfacial polarization effect of hematite nanoparticles. The real and imaginary parts of the electric modulus  $M'$  and  $M''$  can be calculated as follow

$$M' = \frac{\epsilon'}{\epsilon'^2 + \epsilon''^2} \quad \text{and} \quad M'' = \frac{\epsilon''}{\epsilon'^2 + \epsilon''^2}$$

Figures 7(a) and 7(b) show the variation of the electric modulus (real and imaginary) as a function of frequency. It is obvious to underline the real of modulus increases with increasing frequency.

The imaginary part of the electric modulus attained almost constant value except 100°C curve. An increase in both  $M'$  and  $M''$  has been observed at high frequencies and reaches at maximum values. These results can be related to the deficiency of the restoring force governing the mobility of charge carriers under the action of an induced electric field.

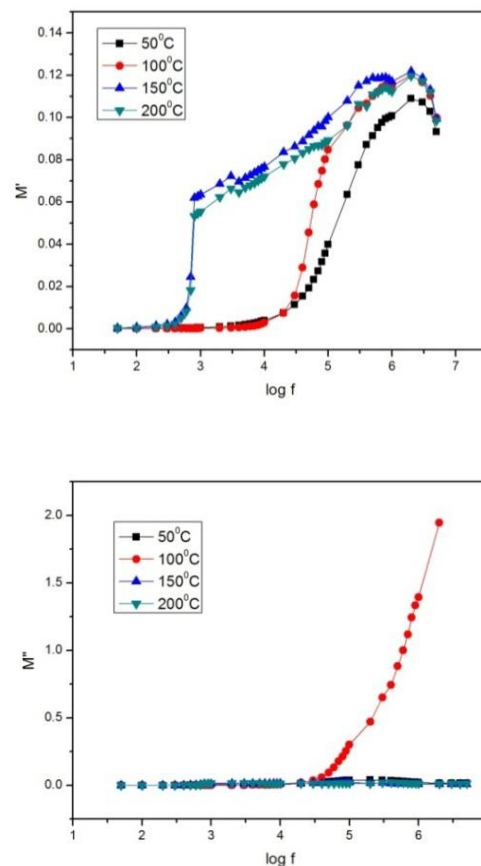


Figure 7: (a) Variation of real part and (b) imaginary part of electric modulus with frequency

### 4. CONCLUSION

Hematite nanoparticles were successfully synthesized by hydrothermal method. X-ray diffraction data confirmed that the synthesized nanoparticles are crystallized in hexagonal crystal system with rhombohedral lattice structure. The FTIR spectrum confirmed the two intrinsic stretching vibration bands of Fe-O at 563 and 475 cm<sup>-1</sup>. The

**One Day International Seminar on Materials Science & Technology (ISMST 2017)****4<sup>th</sup> August 2017****Organized by****Department of Physics, Mother Teresa Women's University, Kodaikanal, Tamilnadu, India**

---

dielectric constant and dielectric loss values of  $\alpha$ -Fe<sub>2</sub>O<sub>3</sub> sample decrease with increase in the frequency of the applied signal. The observed increase in the dielectric loss at low frequency region is due to the space charge polarization. At high frequencies, the AC conductivity increases with increase in frequency due to the hopping of charge carriers. The manageable enhancement in AC conductivity and the controllable variations in both dielectric constant and loss make the synthesized materials appropriate as microwave absorption and filler.

**REFERENCES:**

1. W. Hu, N. Qin, G. Wu, Y. Lin, S. Li and D. Bao, J. Am. Chem. Soc., 2012, 134, 14658.
2. A.Hernandez-Valdes, R.A. Zarate, A.I. Martinez, M.I. Pech-Canul, M.A. Garcia-Lobato, R. Villaroel, Vacuum 105 (2014) 26–32.
3. I. Hong, M. Angelucci, R. Verrelli, G.B. Maria, S. Panero, F. Croce, C. Mariani, B.Scrosati, J. Hassoun, J. Power Sources 256 (2014)133–136.
4. S. Wagloehner, J.N. Baer, S. Kureti, Appl. Catal. B: Environ. 147 (2014) 1000–1008.
5. A.S. Teja, P.Y. Koh, Prog. Cryst. Growth Charact. Mater. 55 (2009) 22–45.
6. M.-C. Huang, Ceram. Int. 40 (2014) 10537–10544.
7. H. Liang, W. Chen, Y. Yao, Z. Wang, Y. Yang, Ceram. Int. 40 (2014) 10283–10290.
8. M. Khalil, J. Yu, N. Liu, R.L. Lee, Colloid. Surf. A: Physicochem. Eng.Aspects 453 (2014) 7–12.
9. M. Tadic, D. Markovic, V. Spasojevic, V. Kusigerski, M. Remskar, J. Pirnat, Z. Jagli-cic, J. Alloys Compd. 441 (2007) 291–296.
10. D. Cardillo, M. Tehei, M. Lerch, S. Corde, A. Rosenfeld, K. Konstantinov, Mater. Lett. 117 (2014) 279–282.
11. X. Zhang, Y. Niu, Y. Li, X. Hou, Y. Wang, R. Bai, J. Zhao, Mater. Lett., 99 (2013) 111–114.
12. S. Yang, Y. Xu, Y. Sun, G. Zhang, D. Gao, Cryst. Eng. Comm. 14 (2012) 7915–7921.
13. J. Ma, J. Lian, X. Duan, X. Liu, W. Zheng, J. Phys. Chem. C 114 (2010) 10671–10676.